THE JOURNAL OF PHYSICAL CHEMISTRY B

Article

Finite-Element Model of Interaction between Fungal Polysaccharide and Monoclonal Antibody in the Capsule of Cryptococcus neoformans

Vineet Rakesh, Andrew D. Schweitzer, Oscar Zaragoza, Ruth Bryan, Kevin Wong, Ashim Datta, Arturo Casadevall, and Ekaterina Dadachova

J. Phys. Chem. B, **2008**, 112 (29), 8514-8522• DOI: 10.1021/jp8018205 • Publication Date (Web): 28 June 2008

Finite-Element Model of Interaction between Fungal Polysaccharide and Monoclonal Antibody in the Capsule of *Cryptococcus neoformans*

Vineet Rakesh,[†,‡] Andrew D. Schweitzer,[‡,§,||,⊥] Oscar Zaragoza,[#] Ruth Bryan,[§] Kevin Wong,[†] Ashim Datta,[†] Arturo Casadevall,[∇,○] and Ekaterina Dadachova*[,§,∇]

Department of Biological and Environmental Engineering, Cornell University, Ithaca, New York 14853, Departments of Nuclear Medicine, of Microbiology and Immunology, and of Medicine, Albert Einstein College of Medicine, Bronx, New York 10461, Medical Fellows Program, Howard Hughes Medical Institute, Chevy Chase, Maryland 20815, The Mount Sinai School of Medicine, New York, New York 10029, and Mycology Unit, National Center for Microbiology, Instituto de Salud Carlos III, Madrid, Spain

Received: March 1, 2008; Revised Manuscript Received: May 17, 2008

Many microorganisms such as bacteria and fungi possess so-called capsules made of polysaccharides which protect these microorganisms from environmental insults and host immune defenses. The polysaccharide capsule of *Cryptococcus neoformans*, a human pathogenic yeast, is capable of self-assembly, composed mostly of glucuronoxylomannan (GXM), a polysaccharide with a molecular weight of approximately 2 000 000, and has several layers with different densities. The objective of this study was to model pore-hindered diffusion and binding of the GXM-specific antibody within the *C. neoformans* capsule. Using the finite-element method (FEM), we created a model which represents the in vivo binding of a GXM-specific antibody to a *C. neoformans* cell taking into account the intravenous infusion time of antibody, antibody diffusion through capsular pores, and Michaelis−Menten kinetics of antibody binding to capsular GXM. The model predicted rapid diffusion of antibody to all regions of the capsule where the pore size was greater than the Stokes diameter of the antibody. Binding occurred primarily at intermediate regions of the capsule. The GXM concentration in each capsular region was the principal determinant of the steady-state antibody−GXM complex concentration, while the forward binding rate constant influenced the rate of complex formation in each region. The concentration profiles predicted by the model closely matched experimental immunofluorescence data. Inclusion of different antibody isotypes (IgG, IgA, and IgM) into the modeling algorithm resulted in similar complex formation in the outer capsular regions, but different depths of binding at the inner regions. These results have implications for the development of new antibody-based therapies.

Introduction

Many microorganisms such as bacteria and fungi possess so-called capsules made of polysaccharides which protect these microorganisms from environmental insults and host immune defenses. For example, the polysaccharide capsule of *Cryptococcus neoformans*, a human pathogenic yeast, is considered the main virulence factor of this pathogen.[1] The capsule, which is capable of self-assembly,[2] is composed mostly of glucuronoxylomannan (GXM), a polysaccharide with a molecular weight of approximately 2 000 000 (90−95% of the capsule), with the rest being another polysaccharide, galactoxylomannan (GalXM; 5%), and as well as mannoproteins (less than 1%)[3] (reviewed in refs 4–6). GXM is an acetylated linear polysaccharide[7] composed of mannose trisaccharide units bearing different combinations of β(1,2)-glucuronic acid, β(1,2)-xylose, and β(1,4)-xylose, depending on the serotype and strain.[8] Figure 1 shows the three types of mannose trisaccharide units which have been identified in GXMs of strain H99.[9] Recent reports where the capsule was subjected to γ radiation capable of gradually removing polysaccharide[10] revealed that the capsule consisted of several regions and its density changed according to radial distribution of GXM, becoming denser at the inner regions of the capsule.[11,12] Importantly, those spatial differences were accompanied by antigenic differences between the regions of the capsule, resulting in an increase of the binding affinity of the GXM-specific monoclonal antibody (mAb; a protein molecule with a molecular weight of approximately 150 000) to the polysaccharide from the inner regions of the capsule.

The abililty of mAb's to the capsular polysaccharide to promote opsonization of *C. neoformans*, allowing uptake by phagocytic cells, is the basis of the antibody-based therapy of patients with *C. neoformans* infection that is currently in clinical development.[13] The discovery that the location of GXM-specific antibody binding to the capsule affected the efficacy of antibody in opsonization, combined with the realization that the capsule is structurally complex, suggests a need for a better understanding of the mechanisms by which antibody interacts with capsular polysaccharide. Computational modeling of diffusion and binding of the GXM-specific mAb to the multilayered polysaccharide structure of the *C. neoformans* capsule could enhance our understanding of the antibody interaction with the capsule and might assist in developing better antibody-based therapies of *C. neoformans* infection. We have recently demonstrated the utility of computational modeling using the finite-element method

[†] Cornell University.
[‡] These authors contributed equally to this work.
[§] Department of Nuclear Medicine, Albert Einstein College of Medicine.
[||] Howard Hughes Medical Institute.
[⊥] The Mount Sinai School of Medicine.
[#] Instituto de Salud Carlos III.
[∇] Department of Microbiology and Immunology, Albert Einstein College of Medicine.
[○] Department of Medicine, Albert Einstein College of Medicine.

10.1021/jp8018205 CCC: $40.75
Published on Web 06/28/2008

a)

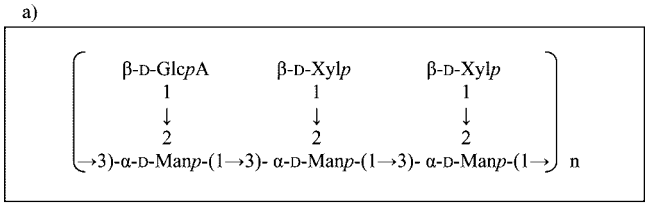

b)

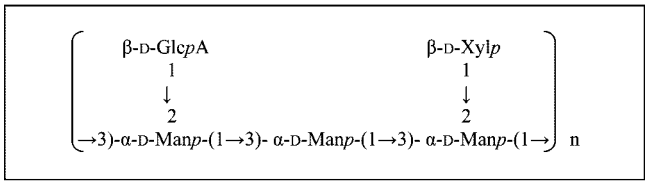

c)

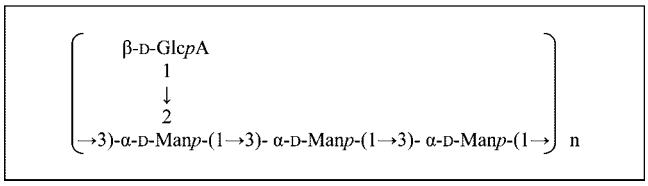

Figure 1. Three mannosyl triads found in GXM of *C. neoformans* strain H99 (serotype A) used in this study: (a) M2, (b) M1, (c) M6. Man*p* represents α-D-mannopyrannan, Glc*p*A represents *β*-D-glucopyranosyluronic acid, and Xyl*p* represents *β*-D-xylopranosyl.

(FEM) in development of antibody-based therapies by modeling the interaction of melanin pigment-binding antibody with tumor melanin.[14] FEM is a powerful method for solving diffusion/binding problems in a three-dimensional geometry. Examples of application of computer modeling to immunological problems on a scale similar to ours include modeling of binding and dissociation kinetics[15] and a concentration gradient immunoassay.[16] Flessner used mass- and volume-balance equations to model diffusion of protein through a deformable porous medium on a scale larger than ours.[17] FEM has also been used to model protein transport in vivo on a microscale,[18] drug delivery in vivo,[19] and even the biochemical reactions occurring within compartments of a single cell.[20] However, to the best of our knowledge, this study is the first attempt to apply computer modeling to the interaction between a microbial polysaccharide capsule and an antibody. In this study the model system was chosen to be a polysaccharide capsule of a *C. neoformans* cell in the plasma of a hypothetical patient during the intravenous infusion of a polysaccharide (GXM)-specific antibody.

The goals of this study were (i) to model the interaction of the antibody with the *polysaccharide* capsule, taking into consideration antibody diffusion through capsular pores and Michaelis−Menten kinetics of antibody binding to capsular GXM, (ii) to identify the factors that limit antibody−antigen complex formation, (iii) to compare the results from the model with experimental immunofluorescence data, (iv) to compare the diffusion and binding characteristics of different antibody isotypes (shown in Figure 2), and (v) to predict which parameters of an antibody are likely to lead to more effective therapy.

Materials and Methods

Governing Equations. The capsule of *C. neoformans* was considered as a spherical shell surrounding the cell body of radius 2.5 μm. It was divided into six different regions with different concentrations of GXM on the basis of the study of Maxson et al.,[11] as shown in Figure 3a. Using a representative *C. neoformans* cell body radius of 2.5 μm, the radii of the capsular regions were calculated from the data of Maxson et al.,[11] which give the thickness of the capsule regions relative to the cell body diameter on the basis of treatment with γ irradiation. Table 1 shows the calculated radii of the different capsular regions.

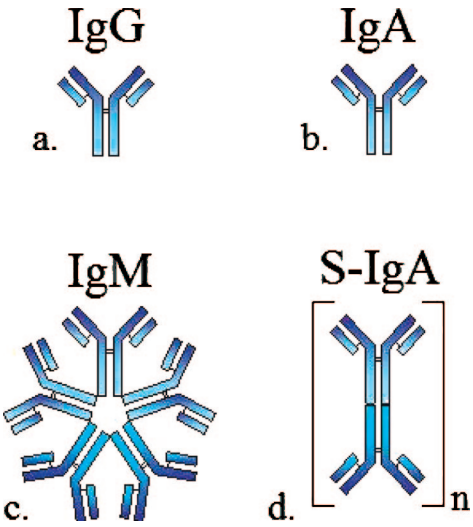

Figure 2. Basic structures of different antibody isotypes: (a) IgG, molecular mass 150 kDa, Stokes diameter 11 nm; (b) monomeric IgA, molecular mass 150 kDa, Stokes diameter 9.4 nm; (c) IgM, molecular mass 970 kDa, Stokes diameter 15 nm; (d) secretory IgA (S-IgA), aggregates of 400 kDa dimers ($n \gg 1$), Stokes diameter 28 nm.

TABLE 1: *C. neoformans* Capsular Region Radii[11]

capsular region; irradiation time (min)	outer radius (μm)	inner radius (μm)	net radius (μm)
1; 0−5	5.35	4.88	0.47
2; 5−10	4.88	4.60	0.28
3; 10−20	4.60	4.47	0.13
4; 20−30	4.47	3.70	0.77
5; 30−40	3.70	3.55	0.15
residual capsule	3.55	2.50	1.05
cell body	0	2.5	2.5

The computational model simulates the process of binding of the GXM-specific mAb 18B7 (IgG1 isotype[13]) as it diffuses inward from the surface of the cell capsule towards the cell wall to the antigen (GXM) present in the capsule. In this model the antibody concentration in the different capsular regions depends on the diffusion of the antibody, formation of the antibody−antigen complex due to the forward reaction, and dissociation of the complex due to the backward reaction and is given by the equation

$$\frac{\partial c_{Ab}}{\partial t} = D_{cap}\frac{1}{r^2}\frac{\partial}{\partial r}\left(r^2\frac{\partial c_{Ab}}{\partial r}\right) - k^f c_{Ab}c_{Ag} + k^b c_{Ab-Ag} \quad (1)$$

Here, c_{Ab}, c_{Ag}, and c_{Ab-Ag} are the antibody, antigen, and complex concentrations, respectively, t is the time, D_{cap} is the diffusivity of the antibody and is different in the different capsular regions, r is the distance from the center of the cell body, and k^f and k^b are the specific rate constant for the forward and backward reactions, respectively.

The antigen concentration in the capsular regions depends on its binding to the free antibody that diffuses into the capsule and on the dissociation of the complex due to the backward reaction

$$\frac{\partial c_{Ag}}{\partial t} = n\left(-k^f c_{Ab}c_{Ag} + k^b c_{Ab-Ag}\right) \quad (2)$$

where n is the valence of the antibody and antigen reaction.

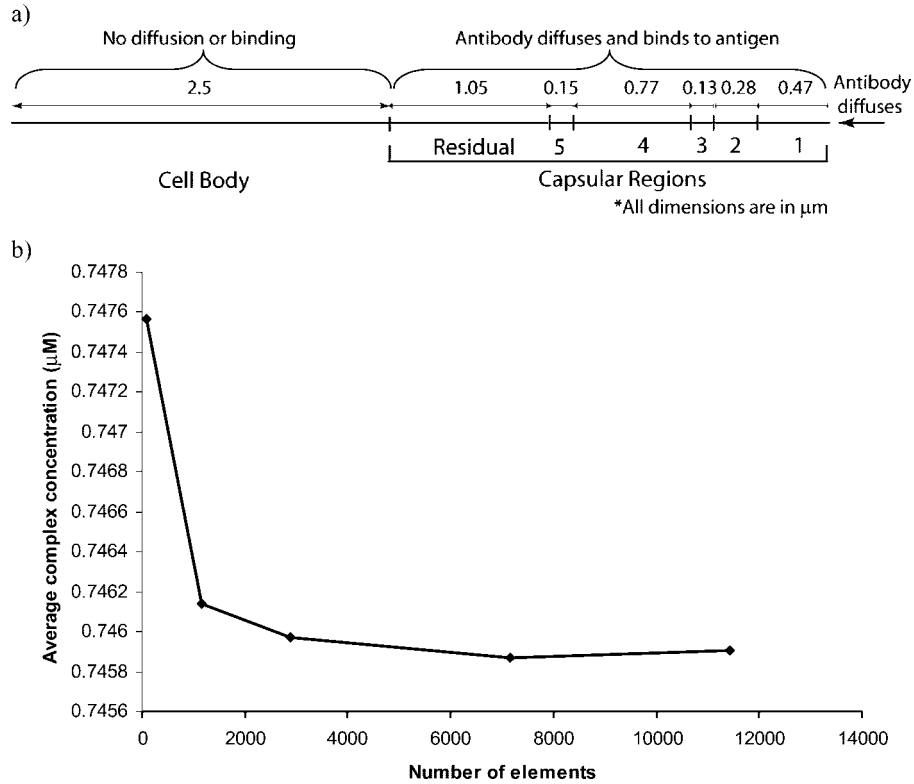

Figure 3. Schematic showing the radial distance from the center of the cell body to the surface of the *C. neoformans* capsule assuming spherical symmetry in the capsule and mesh convergence analysis. (a) Antibody (mAb 18B7) diffuses into the capsule from the outer boundary of the capsule. Different concentrations of the antigen (GXM) are present in the different capsular regions, and the antigen binds to the antibody as diffusion takes place. (b) shows the mesh convergence analysis with the average complex concentration in the capsule at 30 min as the variable. The plot shows no change in the average concentration of the complex when the number of elements used in the finite-element mesh is more than 7153. Therefore, a mesh with 7153 elements was used for all further calculations.

Similarly, the antibody−antigen complex concentration also depends on the forward and backward reactions, and the governing equation is given by

$$\frac{\partial c_{\mathrm{Ab-Ag}}}{\partial t} = k^{\mathrm{f}} c_{\mathrm{Ab}} c_{\mathrm{Ag}} - k^{\mathrm{b}} c_{\mathrm{Ab-Ag}} \tag{3}$$

Boundary Conditions. The concentration of the antibody at the outer boundary (i.e., at $r = 5.35\ \mu$m) of the capsule is given by

$$c_{\mathrm{Ab}r=r_{\mathrm{o}}} = 1.3t\ nM \tag{4}$$

Here t is the time (min). This expression represents the conditions used by Larsen et al.[13] in their phase I clinical trial of mAb 18B7 for antibody-based therapy of *C. neoformans* infection. The maximum tolerated dose (MTD) as determined by the study was 1.0 mg/kg (which would constitute 70 mg for the representative 70 kg patient in our model). In the trial, intravenous infusion of the total dose of 18B7 (70 mg) occurred over 2 h to avoid the possibility of anaphylaxis. Hence, for the first 2 h of therapy, the rate of administration of 18B7 to the plasma was 0.583 mg/min, or 3.89 nmol/min. Assuming a plasma volume of 3 L, the rate of increase of the 18B7 concentration for the first 2 h was 1.30 nM/min. After 2 h, the plasma concentration reached its maximum of 156 nM. Regarding plasma clearance, Larsen et al. found the half-life for the 18B7 in plasma to be 53 h, consistent with the clearance of a mouse IgG1 isotype in humans. Since our model simulates the first 3 h of therapy, the amount of plasma clearance is negligible compared to the high rate of infusion. Therefore, we did not include an expression for plasma clearance in eq 4.

TABLE 2: Antigen (GXM) Concentration in the Different Capsule Regions[11]

capsular region	antigen concn (M)
1	1.59×10^{-6}
2	6.62×10^{-6}
3	1.07×10^{-5}
4	5.88×10^{-5}
5	1.91×10^{-5}
residual	1.91×10^{-5}

The antibody does not diffuse inside the cell body, and hence, at the inner edge of the residual capsule (i.e., at $r = 2.5\ \mu$m), the antibody flux is zero:

$$\frac{\partial c_{\mathrm{Ab}}}{\partial r}_{r=r_i} = 0 \tag{5}$$

Initial Conditions. Initially, there is no antibody or complex in the capsular regions:

$$c_{\mathrm{Ab}t=0} = 0 \tag{6}$$

$$c_{\mathrm{Ab-Ag}t=0} = 0 \tag{7}$$

The antigen concentrations in the different capsular regions were different initially as discussed earlier and shown in Table 2:

$$c_{\mathrm{Ag}t=0} = c_{\mathrm{Ag},0} \tag{8}$$

Solution Details. The governing equations (eqs 1–3) with the boundary and initial conditions given by eqs 4–8 were solved using the FEM. The commercial finite-element solver COMSOL Multiphysics (Comsol Inc., Burlington, MA) was used to obtain

TABLE 3: Antibody Diffusivities in the Different Capsular Regions Calculated from Renkin[21] and Deen[23] [a]

region	outer radius (μm)	inner radius (μm)	estimated pore size (nm)	ratio of the Stokes diameter of the antibody to the pore size	estimated diffusivity based on the pore size from the Renkin equation (cm^2/s)	estimated diffusivity based on the diameter to pore size ratio from Deen (cm^2/s)
1	5.35	4.88	329	0.033	3.82×10^{-7}	3.96×10^{-7}
2	4.88	4.6	161	0.068	3.27×10^{-7}	3.39×10^{-7}
3	4.6	4.47	127	0.087	3.00×10^{-7}	3.12×10^{-7}
4	4.47	3.7	54	0.204	1.64×10^{-7}	1.63×10^{-7}
5	3.7	3.6	46	0.239	1.34×10^{-7}	1.36×10^{-7}
5	3.6	3.55	39	0.282	1.02×10^{-7}	1.06×10^{-7}
RC	3.55	3.5	39	0.282	1.02×10^{-7}	1.06×10^{-7}
RC	3.5	3.4	32	0.344	6.77×10^{-8}	7.04×10^{-8}
RC	3.4	3.3	25	0.440	3.26×10^{-8}	3.52×10^{-8}
RC	3.3	3.2	18	0.611	7.34×10^{-9}	8.80×10^{-9}
RC	3.2	2.5	11	1.000	0	0

[a] Renkin and Deen estimates are based on scaling down the diffusion coefficient of IgG in water, 4.4E−07 cm^2/s.[22] The Stokes diameter of IgG is 11 nm.[22] RC = residual capsule.

TABLE 4: Molecular Mass, Diffusion Coefficients, and Stokes Diameters of Different Human Antibody Isotypes[22]

antibody isotype[a]	molecular mass (Da)	diffusion coefficient in water (cm^2/s)	Stokes diameter (nm)
IgG	150 000	4.4×10^{-7}	11
IgM	970 000	3.2×10^{-7}	15
IgA	150 000	5.2×10^{-7}	9.4
S-IgA	aggregates of 400 000 Da dimers	1.7×10^{-7}	28

[a] IgA represents monomeric IgA, while S-IgA represents aggregates of 400 000 Da dimeric secretory IgA.

TABLE 5: Michaelis−Menten Kinetics Reaction Constants Based on Scatchard Analysis of *C. neoformans* Capsular Regions[11]

capsule region; irradiation time (min)	K_a (M^{-1})	k^b (s^{-1})	k^f (M^{-1} s^{-1})
1; 0−5	2.90×10^8	1.00×10^{-5}	2.90×10^3
2; 5−10	2.90×10^8	1.00×10^{-5}	2.90×10^3
3; 10−20	4.90×10^7	1.00×10^{-5}	4.90×10^2
4; 20−30	5.00×10^7	1.00×10^{-5}	5.00×10^2
5; 30−40	1.20×10^8	1.00×10^{-5}	1.20×10^3
residual capsule	8.00×10^7	1.00×10^{-5}	8.00×10^2

the solution. The input parameters for the model are shown in Tables 1–4 and discussed in detail in the next section. Since the geometry of the *C. neoformans* cell is considered to be spherical and the capsular regions are spherical shells, the problem can be reduced to one dimension using the governing equations in the spherical coordinate system as shown in eqs 1–3. The reduction of the problem to one dimension saves significant computational resources without a consequent loss of generality. The geometry of the domain used for the calculation is, therefore, a line divided into different parts representing the different capsular regions and is shown in Figure 3a. Capsular region 5 and the residual capsule were further divided into smaller parts to account for different values of antibody diffusivities (as shown in Table 3) in these regions depending on the distance from the cell center. Transient diffusion equations with source terms for the forward and backward reactions were used to implement eqs 1–3 in the solver (COMSOL Multiphysics). To obtain the antigen and complex concentrations (eqs 2 and 3), the diffusivities of GXM were set to zero in the solver as GXM is part of the polysaccharide matrix of the capsule and is thus relatively immobile.

In FEM, the geometry of the model is divided into smaller regions known as elements. Elements are defined by a set of points known as nodes, and the governing equations are solved at these nodes. The mesh is the collection of elements. Mesh convergence analysis refers to the process of running simulations with a varying number of elements to ensure that the solution is not erroneous due to a lack of mesh precision and was performed for this purpose. The average complex concentration after 30 min was obtained for different mesh densities and plotted as a function of the number of elements in the mesh (as shown in Figure 3b). It was observed that the average complex concentration in the capsule did not change if the number of elements in the mesh was increased beyond 7153. Therefore, all subsequent calculations were done with 7153 elements in the mesh. The simulations were done on a 3.6 GHz Pentium 4 Windows workstation with 2 Gb of RAM.

Input Parameters. The input parameters used for the simulations are shown in Tables 1–5.

Capsular Region Radii. Maxson et al.[11] described that the gradual release of *C. neoformans* capsular polysaccharide after γ irradiation occurred in a dose-dependent manner. By irradiating *C. neoformans* cells for different times, they defined different capsular regions and expressed the thickness of each region relative to the cell body diameter. Using these data, we calculated the radius of each of the capsular regions on the basis of a representative cell body radius of 2.5 μm. Table 1 shows the calculated radii of the different capsular regions, corresponding to the duration of irradiation. The "residual capsule" was the remaining capsule surrounding the cell body after 40 min of irradiation.

Antigen Concentrations in the Different Capsular Regions. Table 2 shows the antigen concentration in the different capsular regions. These were also obtained from the data of Maxson et al.[11]

Antibody Diffusivities in the Capsular Regions. The antibody diffusivities in the different capsular regions were calculated using a semiempirical equation from Renkin:[21]

$$\frac{D_{ig}}{D_{iw}} = \left(1 - \frac{2R_S}{D_p}\right)^2\left[1 - 2.104\left(\frac{2R_S}{D_p}\right) + 2.09\left(\frac{2R_S}{D_p}\right)^3 - 0.95\left(\frac{2R_S}{D_p}\right)^5\right] \quad (9)$$

where D_{ig} is the diffusivity of IgG in a cellulose gel of given pore size, D_{iw} is the diffusivity of IgG in water, R_S is the Stokes

radius of IgG (=5.5 nm, from Saltzman et al.[22]), and D_p is the pore diameter. Diffusivities were also calculated using data from Deen[23] and used in the analysis to determine that the results were independent of the method used for calculating the diffusivity. Diffusivities for IgM, monomeric IgA, and S-IgA were determined using the same method; Stokes radii and diffusivities in water were also from Saltzman et al.[22]

Estimation of the Pore Diameter. To estimate the pore diameter, we combined several methods, on the basis of the available published data. The overall goal was to represent the molecular sieving exhibited by the *C. neoformans* capsule, which has been demonstrated in prior studies.[5,24] Data on exclusion zones of dextrans of various molecular masses were published by Gates et al.,[24] who found that a 70 kDa dextran only diffused within 0.7 μm of the cell wall (3.2 μm from the center of the cell in our model), while a 200 kDa dextran only diffused to within 1.3 μm of the cell wall (3.8 μm from the center). Stokes radii for these dextrans were taken from the literature; a 70 kDa dextran has a 5.5 nm Stokes radius,[25] and a 200 kDa dextran has a 27 nm Stokes radius.[26] Since molecules no longer diffuse when the Stokes diameter is greater than or equal to the pore diameter, we concluded that, at 0.7 μm from the cell wall (3.2 μm radius), the pore diameter is 11 nm and that, at 1.3 μm from the cell wall (3.8 μm radius), the pore diameter is 54 nm. The pore diameter was assumed to change linearly, a gradient was calculated between 3.2 and 3.8 μm, and the pore diameter was assumed to be 54 nm up to a radius of 4.47 μm. From 4.47 to 5.35 μm, no experimental data were found that could directly estimate the pore diameter, so the known relationship[22] was used:

$$D_p \propto \frac{1}{\sqrt{c}} \tag{10}$$

where c represents the concentration of GXM.

Using these pore diameters, diffusivities were calculated using eq 9 and are provided in Table 3. Diffusivities for isotypes IgM, IgA, and S-IgA were calculated in the same manner, with differing Stokes radii and diffusivities in water shown in Table 4 (calculated diffusivities of each isotype at each radius not shown).

Michaelis−Menten Kinetics Reaction Constants. Table 5 shows the values of the rate constants for the forward and backward reactions for binding of 18B7 mAb to GXM, determined using Scatchard analysis by Maxson et al.[11]

Experimental Determination of Antibody Binding within the Capsule. Immunofluorescence was performed after labeling of the capsule of 10^6 cryptococcal cells with calcofluor (50 μg/mL) and FITC-conjugated 18B7 (3 μg/mL). Emissions within the wavelength ranges of 410−480 nm (calcofluor) and 495−535 nm (FITC) were visualized using a Leica AOBS laser scanning confocal microscope.

Results and Discussion

The Model Predicts Rapid Diffusion of Antibody to All Regions of the Capsule Where the Pore Size Is Greater Than the Stokes Diameter of the Antibody. Figure 4 shows the antibody, antigen, and complex concentrations in the capsule as a function of the distance from the cell center at 0, 30, 60, 90, 120, 150, and 180 min using antibody diffusivities calculated from the semiempirical equation from Renkin[21] (eq 9). No appreciable difference in the concentration profiles was observed between Renkin's equation versus Deen's data[23] (plots not shown). Therefore, we concluded that the small change in the diffusivity values obtained by the two methods (Table 3) does not change the results. Hence, the equation from Renkin was used for all subsequent simulations.

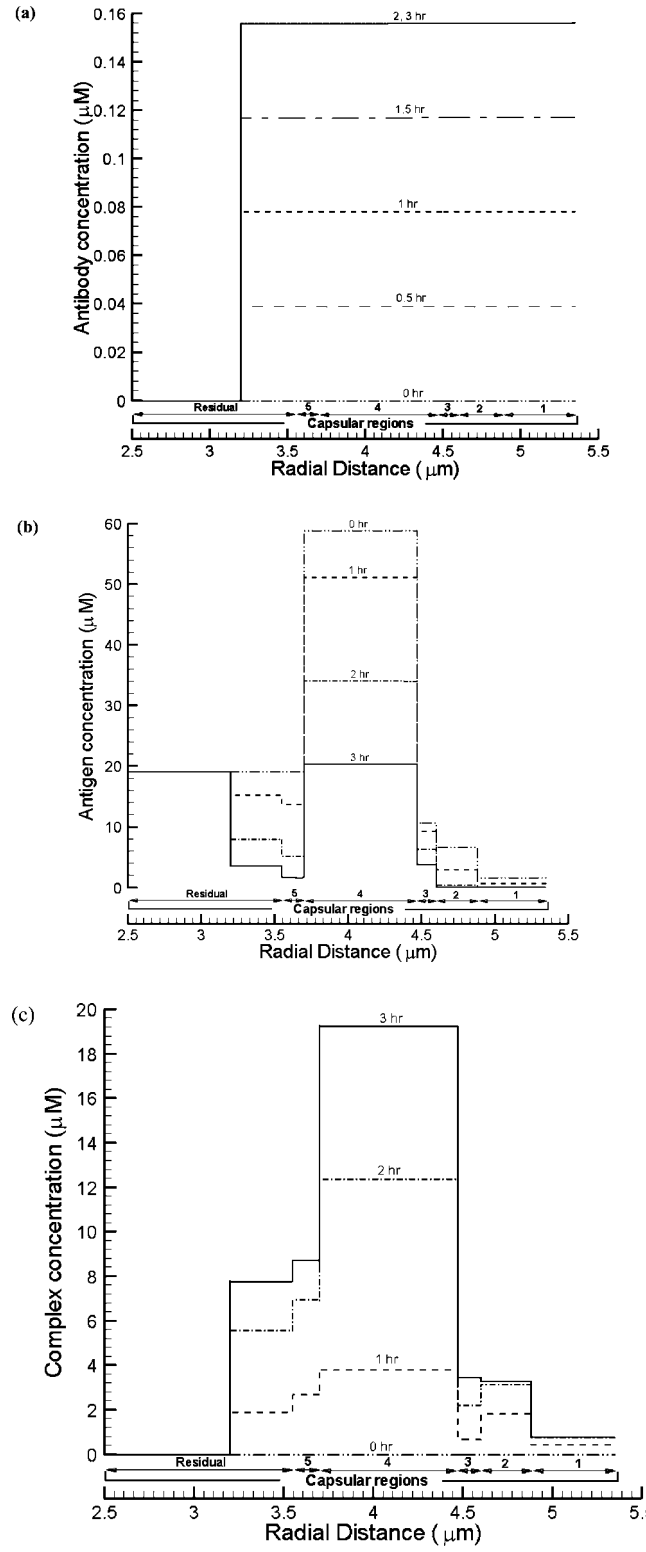

Figure 4. Antibody, antigen, and complex concentrations in the capsule vs radial distance from the cell center at different times using antibody diffusivities calculated using the equation from Renkin (eq 9): (a) antibody, (b) antigen, (c) complex. The total dose of antibody is administered intravenously over the first 2 h.

Figure 5 shows that the diffusion of the antibody from the outside of the capsule to the interior takes place within 0.5 s after the start of antibody infusion. This surprising result can be explained by the scale of the model; diffusion only needs to

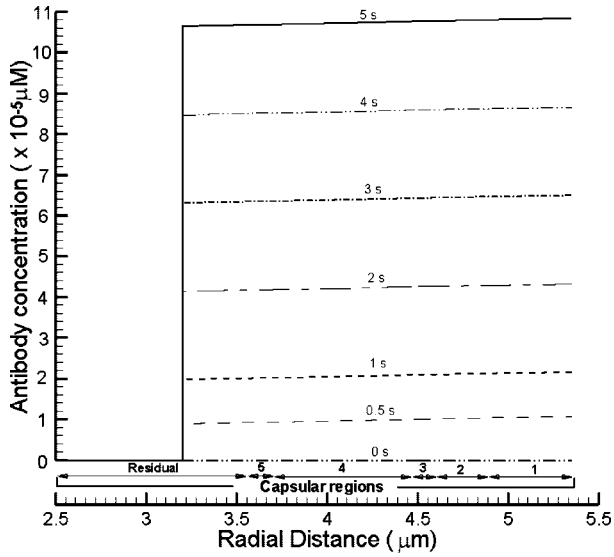

Figure 5. Antibody concentration in the capsule vs radial distance from the cell center at 0, 0.5, 1, 2, 3, 4, and 5 s using antibody diffusivities calculated using a semiempirical equation (eq 9).

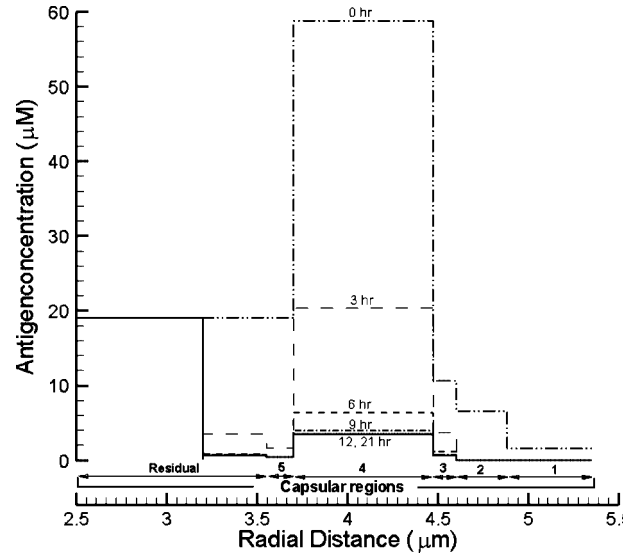

Figure 6. Antigen concentration in the capsule vs radial distance from the cell center at 3, 6, 12, 15, 18, and 21 h. The total dose of antibody is administered intravenously over the first 2 h.

occur over the microscopic radial distance of 2.15 μm to reach 0.7 μm from the cell wall, where the Stokes diameter of the antibody is equal to or greater than the pore diameter, beyond which no diffusion occurs. The equal antibody concentration throughout the capsule at each time point illustrates that any diffusion gradient of the antibody concentration within the capsule only exists for a fraction of a second. Rapid diffusion is also illustrated by the finding that, as free antibody is consumed during binding at different rates in each capsular region, additional antibody diffuses almost immediately from the adjacent capsular regions and the outside, maintaining a flat concentration profile in the capsule.

Another way to explain the rapid diffusion is through a dimensionless quantity called the Thiele modulus, which is used to classify chemical processes involving diffusion and reaction kinetics. The Thiele modulus is a measure of the relative rates of reaction and diffusion.[27] It is defined for this study as

$$\varphi = \delta\sqrt{\frac{k^{b}}{D_{cap}}} \tag{11}$$

where ϕ is the Thiele modulus and δ is the thickness of the different capsular layers. The backward reaction has been taken as the reference to define the Thiele modulus. By definition, a large value of the Thiele modulus corresponds to a process in which diffusion is rate-limiting whereas a small value of the Thiele modulus corresponds to a process where reaction is rate-limiting. In this study, the Thiele moduli for the different capsular layers where diffusion occurs are in the range of 4.9×10^{-5} to 6×10^{-4}, which are very small.[28] This again shows that this process does not have diffusion limitations.

Figure 4b shows the free antigen (GXM) concentration as a function of time in the different capsular regions, which have different initial antigen concentrations (Table 2). Antibody−antigen complex formation in the first 3 h after the start of antibody infusion results in the free antigen concentration falling to almost zero in regions 1 and 2 and to low values in regions 3 and 5 and the residual capsule. However, a significant amount of antigen remains in region 4, which had the highest initial antigen concentration.

Complex Formation in Each Region Is Determined by the Forward Binding Reaction and GXM Concentration. Figure 4c shows the antibody−antigen complex concentration as a function of the distance from the cell center at different times. Since the concentration of free antibody is the same in all capsular regions at any given time (Figure 4a), the amount of complex formed in each region depends entirely on the free antigen concentration and the binding rate constant in that region. To determine the relative importance of these two factors, regions 2 and 4 can be compared. While the initial antigen concentration is 8.9 times higher in region 4 than in region 2 (Table 2), the forward binding rate constant is 5.8 times higher in region 2 than in region 4 (Table 4). It is observed (from Figure 4c) that region 4 has the highest complex concentration at all times used in the simulation. Therefore, while the forward rate constants play an important role in determining the rate at which binding occurs, the availability of more antigen binding sites drives the binding reaction forward more significantly. In addition, as is seen in Figure 4, the initial antigen concentration is the major determinant of the steady-state complex concentration. The last region to reach equilibrium is region 4, and this occurs 12 h after the start of infusion (Figure 6). For the region of the residual layer with the distance from the cell center less than 3.2 μm, no complex is formed as the antibody does not diffuse in the layer; again, this is due to the Stokes diameter of the antibody exceeding the pore diameter.

Concentration Profiles Determined Experimentally Match the Model Prediction. We evaluated the predictions of the model by using fluorescently labeled mAb 18B7, which allowed visualization of the spatial distribution of antibody bound in the capsule (Figure 7). The concentration profiles predicted by the model were superimposed on the immunofluorescence-derived curves by proportionally scaling up the model prediction to match the experimental capsule thickness. Implicit in this method of superimposition is the assumption that while the capsule thickness can vary significantly from cell to cell in the same population of *C. neoformans*, the capsular regions (which are characterized by different GXM concentrations, rate constants, etc.) remain in the same proportions as those reported by Maxson et al.[11] The fluorescence intensity measured for antibody bound to the capsule matched the complex concentration predicted by the model well. One notable difference between the model and experimental results is that the peak complex concentration predicted by the model was located somewhat deeper in the capsule than observed experimentally.

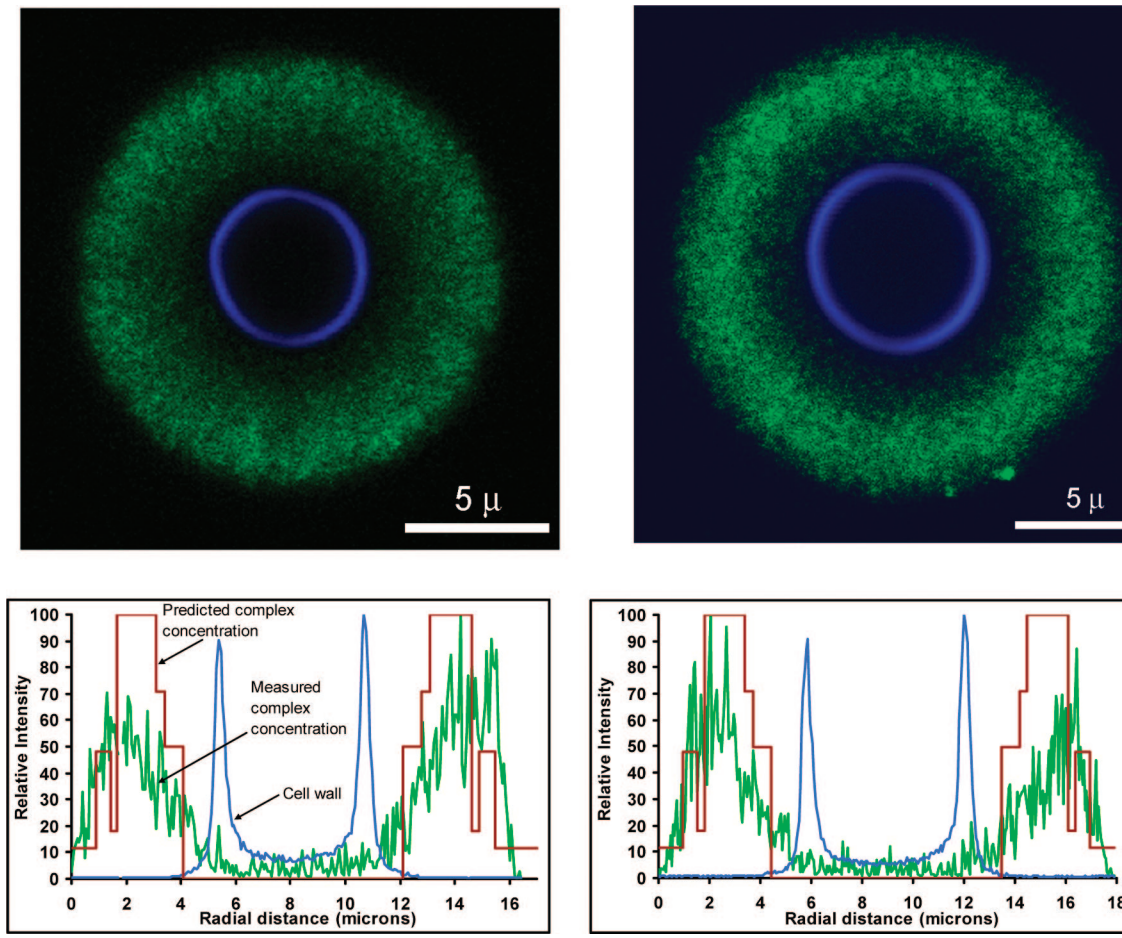

Figure 7. Comparison of model prediction with experimental results obtained for *C. neoformans* cells using immunofluorescence. Green shows the concentration of the complex. The boundaries of the cell wall are shown in blue, detected using calcoflour. Shown are data for two cell sizes.

There are several possible reasons for this. First, although both the model and the experiment allowed 1 h for binding to occur, modeling predicted in vivo events, while the experiment was performed in vitro, where antibody was depleted as diffusion and binding occurred. Second, the assumption made above that the capsule regions each maintained constant proportions as the capsule thickness was varied may not be valid. That is, in cells with smaller capsules one capsular region may predominate, while in cells with larger capsules another region could predominate. Third, steric hindrance from antibody that has bound to a GXM motif at the surface of a pore could decrease the effective pore size. Finally, as binding occurs, antibody cross-linking may reduce the effective pore size and impede diffusion of the antibody to deeper sites.[29]

Interestingly, the model predicts a peak concentration in region 2, followed by a dip in region 3. This is due to a higher binding rate constant in region 2 than in region 3, resulting in a significant difference at the early time of 1 h (since we are comparing to an experiment where binding was allowed to occur for 1 h). However, after 3 h, the concentration in region 3 is predicted to exceed that of region 2, reflecting that the antigen concentration is the major determinant of the steady-state complex concentration, as discussed above.

At the innermost regions of the capsule, the model predicts an abrupt decrease in complex concentration, which reflects the point where the antibody Stokes diameter begins to exceed the decreasing pore sizes. However, experimentally, a gradual decrease to the cell wall is noted. This difference can be explained by biological variation that cannot be modeled, such that at a particular radial distance there is a distribution of pore sizes, whereas the model can only account for an average pore size. Therefore, even in regions where the average pore size is less than the Stokes radius of the antibody, there will be some pores which will be large enough for antibody to pass through.

Different Antibody Isotypes (IgM, IgA, and S-IgA) Result in Similar Complex Formation at the Outer Capsular Regions, but IgA and S-IgA Result in Different Depths of Binding at the Inner Regions. Figure 8 shows the antibody, antigen, and complex concentrations after 3 h for IgM, monomeric IgA, and aggregates of S-IgA. The complex concentration profile of IgM was the same as that of IgG, owing to their similar diffusivities and Stokes radii. Of note, had the model been more precise with regard to the pore diameters, we would expect the depth of IgM binding to be slightly less than that of IgG, as their respective Stokes diameters are 15 and 11 nm. The smaller Stokes diameter of monomeric IgA resulted in diffusion all the way through the residual capsule to the cell wall. Conversely, the larger Stokes diameter of S-IgA resulted in a decreased depth of binding. In addition, the lower diffusivity of S-IgA resulted in a nonsignificant decrease in the complex concentration in capsular regions 4 and 5 (Figure 8).

Sensitivity Analysis. Finally, sensitivity analyses were performed by running a simulation for the case when the entire dose of antibody is given as an intravenous bolus (instantly). The model predictions for this case did not differ qualitatively from the predictions for the 2 h long infusion. Figure 9 shows

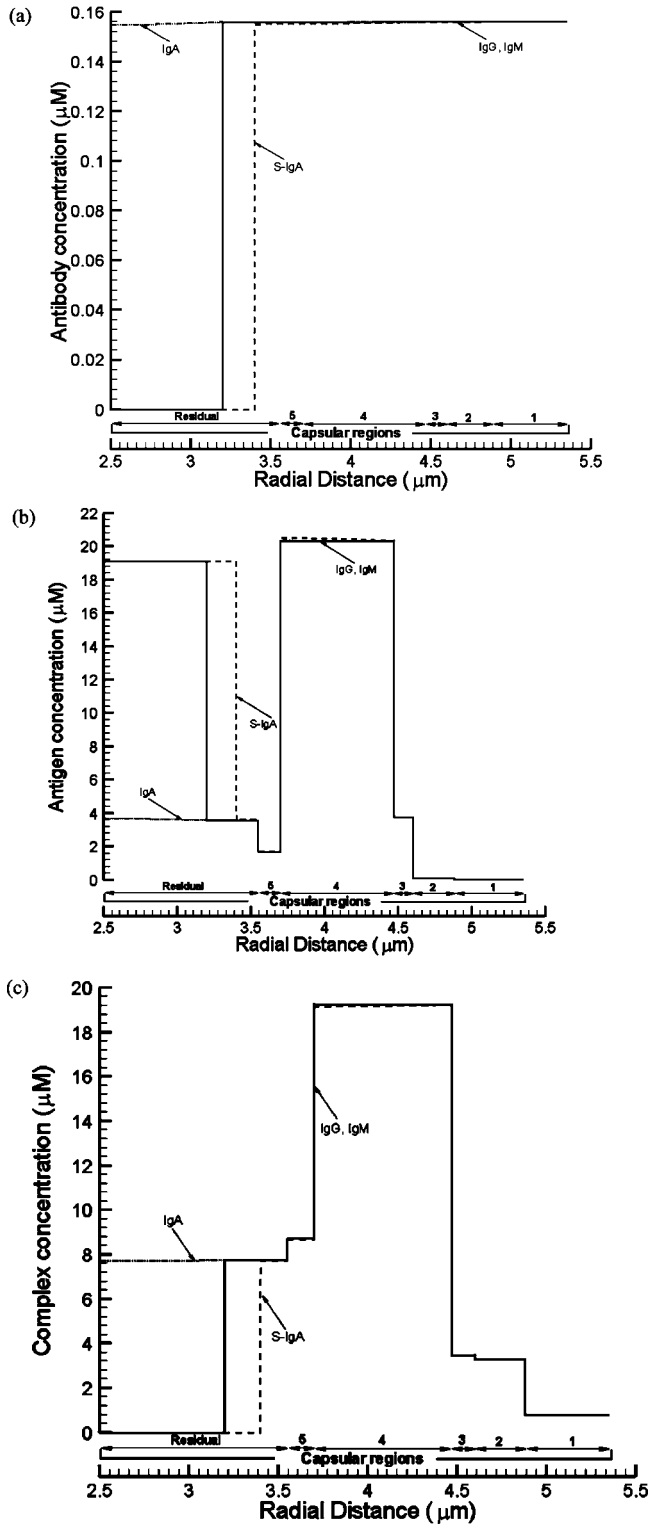

Figure 8. Antibody, antigen, and complex concentrations as a function of the radial distance for IgG, IgM, IgA, and S-IgA antibodies after 3 h: (a) antibody, (b) antigen, (c) complex.

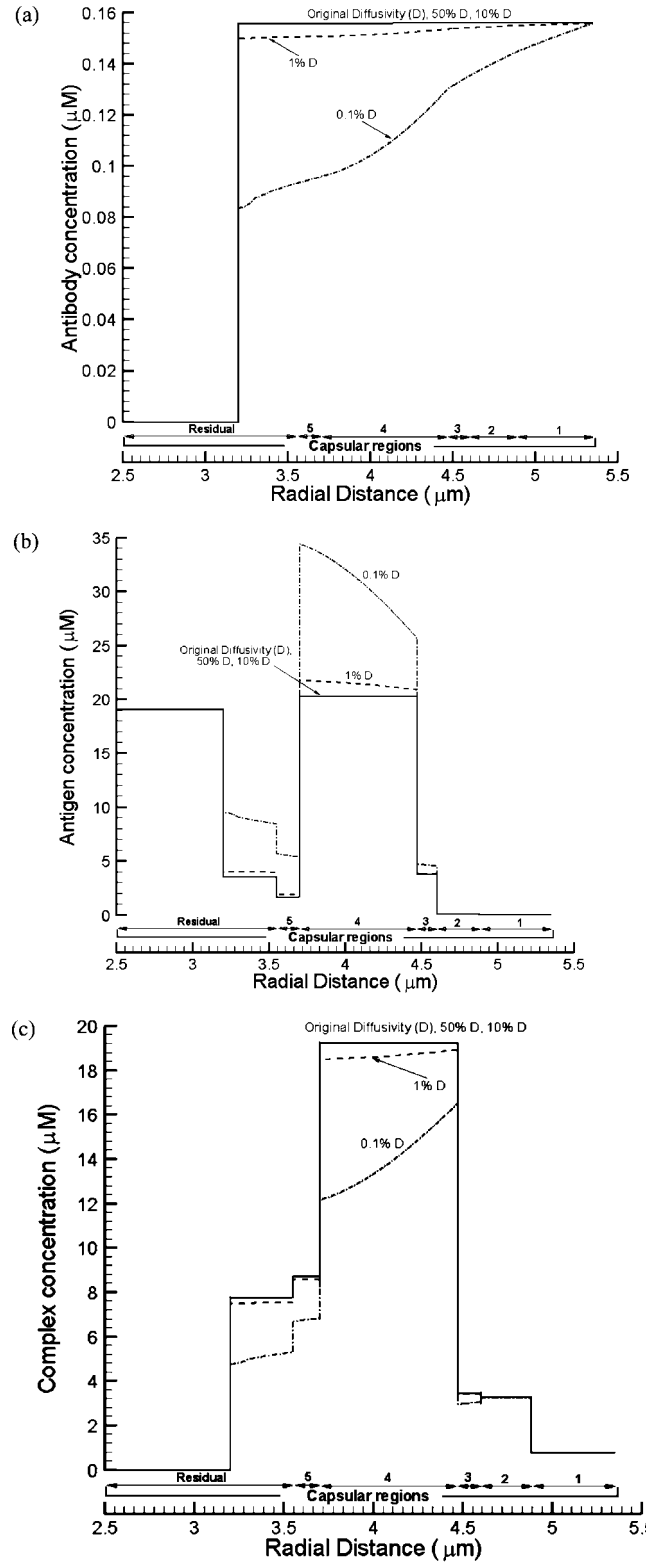

Figure 9. Antibody, antigen, and complex concentrations as a function of the radial distance for different antibody diffusivity values after 3 h: (a) antibody, (b) antigen, (c) complex. The different antibody diffusivity values used were 0.5, 0.1, 0.01, and 0.001 times the original diffusivity.

the antibody, antigen, and complex concentrations for 50%, 10%, 1%, and 0.1% of the original diffusivity. Only a minor concentration gradient in the antibody concentration profile is present at 1%, whereas a significant gradient is observed at 0.1% of the original diffusivity. Therefore, the previously mentioned "sealing" of the capsule is likely to decrease the diffusivity by at least 1000-fold. In the case of region 4, such a decrease in diffusivity would be caused by the pore size decreasing from 54 to 12 nm (just 1 nm greater than the Stokes diameter of IgG). Therefore, either antibody steric hindrance from binding or the putative antibody cross-linking must be extensive enough to significantly decrease the pore size, even at more superficial regions of the capsule where the pore size is much larger.

The location of antibody binding in the capsule is critical for opsonic efficacy since antibody bound deep within the

capsule would not be able to interact with Fc receptors and mediate phagocytosis. Hence, the model results combined with the immunoflourescence results suggest that much of the antibody bound by the capsule is sequestered at sites distant from the capsule surface at a distance that seems to preclude interaction with Fc receptors. Consequently, the size of the capsule is likely to affect the efficacy of antibody by virtue of its large capacity for binding antibody in regions that are ineffective for opsonization.

Conclusions

We mathematically modeled the polysaccharide (GXM)-specific antibody diffusion and binding to the multilayered polysaccharide capsule of a *C. neoformans* cell during antibody infusion into the blood stream. The concentration profiles predicted by the model closely matched experimental immunofluorescence data. The model predicted rapid diffusion of antibody to all regions of the capsule where the pore size was greater than the Stokes diameter of the antibody. Binding occurred primarily at intermediate regions of the capsule. The GXM concentration in each capsular region was the principal determinant of the steady-state antibody−GXM complex concentration, while the forward binding rate constant influenced the rate of complex formation in each region. Different antibody isotypes resulted in similar complex formation in the outer capsular regions, but different depths of binding at the inner regions. These results have implications for the development of new antibody-based therapies.

Acknowledgment. A.D.S. is a Howard Hughes Medical Institute Medical Research Training Fellow. E.D. was supported by NIH Grant AI60507; A.C. was supported by NIH Grants AI33774, HL59842, AI33142, and AI52733. The research was partially supported by internal funds from Cornell University (A.D. and V.R.).

References and Notes

(1) Casadevall, A.; Steenbergen, J. N.; Nosanchuk, J. D. *Curr. Opin. Microbiol.* **2003**, *6*, 332–337.

(2) Nimrichter, L.; Frases, S.; Cinelli, L. P.; Viana, N. B.; Nakouzi, A.; Travassos, L. R.; Casadevall, A.; Rodrigues, M. L. *Eukaryotic Cell* **2007**, *6*, 1400–1410.

(3) Reiss, E.; Cherniak, R.; Eby, R.; Kaufman, L. *Diagn. Immunol.* **1984**, *2*, 109–115.

(4) Bose, I.; Reese, A. J.; Ory, J. J.; Janbon, G.; Doering, T. L. *Eukaryotic Cell* **2003**, *2*, 655–663.

(5) Doering, T. L. *Trends Microbiol.* **2000**, *8*, 547–553.

(6) McFadden, D. C.; Casadevall, A. *Med. Mycol.* **2001**, *39* (1), 19–30.

(7) Cherniak, R.; Sundstrom, J. B. *Infect. Immun.* **1994**, *62*, 1507–1512.

(8) Cherniak, R.; Valafar, H.; Morris, L. C.; Valafar, F. *Clin. Diagn. Lab. Immunol.* **1998**, *5*, 146–159.

(9) McFadden, D. C.; Fries, B. C.; Wang, F.; Casadevall, A. *Eukaryotic Cell* **2007**, *6*, 1464–1473.

(10) Bryan, R. A.; Zaragoza, O.; Zhang, T.; Ortiz, G.; Casadevall, A.; Dadachova, E. *Eukaryotic Cell* **2005**, *4*, 465–475.

(11) Maxson, M. E.; Dadachova, E.; Casadevall, A.; Zaragoza, O. *Eukaryotic Cell* **2007**, *6*, 95–109.

(12) Maxson, M. E.; Cook, E.; Casadevall, A.; Zaragoza, O. *Fungal Genet. Biol.* **2007**, *44*, 180–186.

(13) Larsen, R. A.; Pappas, P. G.; Perfect, J.; Aberg, J. A.; Casadevall, A.; Cloud, G. A.; James, R.; Filler, S.; Dismukes, W. E. *Antimicrob. Agents Chemother.* **2005**, *49*, 952–958.

(14) Schweitzer, A. D.; Rakesh, V.; Revskaya, E.; Datta, A.; Casadevall, A.; Dadachova, E. *Melanoma Res.* **2007**, *17*, 291–303.

(15) Glaser, R. W. *Anal. Biochem.* **1993**, *213*, 152–161.

(16) Foley, J. O.; Nelson, K. E.; Mashadi-Hossein, A.; Finlayson, B. A.; Yager, P. *Anal. Chem.* **2007**, *79*, 3549–3553.

(17) Flessner, M. F. *Am. J. Physiol.: Gastrointest. Liver Physiol.* **2001**, *281*, 424–437.

(18) Sadegh Zadeh, K.; Elman, H. C.; Montas, H. J.; Shirmohammadi, A. *Biomed. Eng. Online* **2007**, *6*, 24.

(19) Weinberg, B. D.; Patel, R. B.; Exner, A. A.; Saidel, G. M.; Gao, J. *J. Controlled Release* **2007**, *124*, 11–19.

(20) Ladik, J. *Int. J. Quantum Chem.* **2006**, *106*, 2827–2832.

(21) Renkin, E. M. *J. Gen. Physiol.* **1954**, *38*, 225–243.

(22) Saltzman, W. M.; Radomsky, M. L.; Whaley, K. J.; Cone, R. A. *Biophys. J.* **1994**, *66*, 508–515.

(23) Deen, W. M. *AIChE J.* **1987**, *33*, 1409–1425.

(24) Gates, M. A.; Thorkildson, P.; Kozel, T. R. *Mol. Microbiol.* **2004**, *54*, 13–24.

(25) Lang, I.; Scholz, M.; Peters, R. *J. Cell Biol.* **1986**, *102*, 1183–1190.

(26) Chua, B. A.; Perks, A. M. *J. Physiol.* **1998**, *513*, 283–294.

(27) Fogler, H. S. *Elements of Chemical Reaction Engineering*; Prentice Hall, Inc.: Upper Saddle River, NJ, 1986.

(28) Stewart, P. S.; Raquepas, J. B. *Chem. Eng. Sci.* **1995**, *50*, 3099–3104.

(29) Zaragoza, O.; Casadevall, A. *Cell Microbiol.* **2006**, *8*, 1862–1876.

JP8018205